Biophysical *Journal*
Article

Biophysical Society

Curcumin Dictates Divergent Fates for the Central Salt Bridges in Amyloid-β_{40} and Amyloid-β_{42}

Bappaditya Chandra,[1] Venus Singh Mithu,[2] Debanjan Bhowmik,[1] Anand Kant Das,[1] Bankanidhi Sahoo,[3] Sudipta Maiti,[1,*] and Perunthiruthy K. Madhu[1,3,*]

[1]Department of Chemical Sciences, Tata Institute of Fundamental Research, Colaba, Mumbai, India; [2]Department of Chemistry, Guru Nanak Dev University, Amritsar, India; and [3]TIFR Centre for Interdisciplinary Sciences, Tata Institute of Fundamental Research, Narsinghi, Hyderabad, India

ABSTRACT There are three specific regions in the Amyloid beta (Aβ) peptide sequence where variations cause enhanced toxicity in Alzheimer's disease: the N-terminus, the central salt bridge, and the C-terminus. Here, we investigate if there is a close conformational connection between these three regions, which may suggest a concerted mechanism of toxicity. We measure the effects of Zn^{2+} and curcumin on Aβ_{40}, and compare these with their previously reported effects on Aβ_{42}. Aβ_{42} and Aβ_{40} differ only near the C-terminus, where curcumin interacts, while Zn^{2+} interacts near the N-terminus. Therefore, this comparison should help us differentiate the effect of modulating the C- and the N-termini. We find that curcumin allows fibril-like structures containing the salt bridge to emerge in the mature Aβ_{40} aggregates, but not in Aβ_{42}. In contrast, we find no difference in the effects of Zn^{+2} on Aβ_{40} and Aβ_{42}. In the presence of Zn^{+2}, both of these fail to form proper fibrils, and the salt bridge remains disrupted. These results indicate that modulations of the Aβ termini can determine the fate of a salt bridge far away in the sequence, and this has significant consequences for Aβ toxicity. We also infer that small molecules can alter oligomer-induced toxicity by modulating the aggregation pathway, without substantially changing the final product of aggregation.

INTRODUCTION

Toxicity associated with amyloid beta (Aβ) aggregation is linked to Alzheimer's disease (1–4), but the mechanism of toxicity has remained unknown. Nature provides indications that Aβ toxicity has a structural origin. For example, Aβ_{40} and Aβ_{42} are the two major isoforms of Aβ found in the brain plaques of Alzheimer's patients. They are identical except for the two extra amino acids at the C-terminus of Aβ_{42}, which make it fold differently (5–9), and also make it more aggregation-prone and toxic (10). At least two other regions also seem to be important for determining toxicity. Mutations in Aβ that lead to early onset AD almost exclusively map to one of these two regions: the N-terminus (first seven residues, which are loosely structured at best); or the central region (residues 21–23) (11–13), which in wild-type Aβ_{40}, contains a salt bridge. It is interesting to hypothesize that these three regions constitute conformationally connected arms of the same toxic mechanism.

Curcumin, a biphenolic compound known to interact with Aβ and alter its properties (14–18), provides a natural handle to test this hypothesis. Curcumin is known to modulate Aβ toxicity (17,19,20), and its most prominent site of interaction is the C-terminal region, though it also interacts with some residues at the N-terminal region (as shown for Aβ_{42} (21,22)). Zn^{2+}, another well-known modulator of Aβ aggregation and toxicity (23,24), provides an ideal comparison. It is thought to interact almost exclusively with the Histidine residues near the N-terminal (25–27). It therefore should have very similar effects on Aβ_{42} and Aβ_{40}. Both Zn^{2+} and curcumin are known to interact with the toxic oligomers of Aβ_{42}, and sequester them by accelerating their precipitation, which yield similar nonfibrillar aggregates. Significantly, the salt bridge between Lys^{28} and Asp^{23}, a key structural feature of mature C-terminal-amidated Aβ fibrils (28), is lacking in these Aβ_{42} aggregates (21,29). It was inferred that these agents disrupt the salt bridge. Notably, a large fraction of the mutations associated with early onset AD occurs in the two neighboring residues

Submitted November 4, 2016, and accepted for publication February 7, 2017.

*Correspondence: maiti@tifr.res.in or madhu@tifr.res.in

Debanjan Bhowmik's present address is Department of Chemistry, Northwestern University, Evanston, Illinois.

Anand Kant Das's present address is Vienna University of Technology, Institute for Applied Physics - Biophysics group, Vienna, Austria.

All animal experimental protocols were approved by the Institute Animal Ethics committee.

Editor: Francesca Marassi.

http://dx.doi.org/10.1016/j.bpj.2017.02.043

(E22 and D23) in the salt-bridge region (13). We note that recent works on two different preparations of the Aβ_{42} fibril have suggested a different salt bridge between K28 and the terminal carboxylate (9,30). However, in alternative preparations, such as those where the C-terminal is amidated, Lys^{28} does form a salt bridge with D23 (29). In addition, we have also shown that there are significant structural differences between the transient toxic oligomers and the less toxic mature fibrils of Aβ_{40} in the salt-bridge region (1). Hence, the perturbation of the salt bridge may be directly linked to the alteration of toxicity.

The above-mentioned reports suggested that the terminal regions of Aβ_{42} can control the fate of the central salt bridge, but they could not rule out direct involvement of Zn^{2+} or curcumin with the central region. However, if the effect of curcumin on the salt bridge is different for Aβ_{40} and Aβ_{42}, then it will strongly indicate that the state of the residues at the C-terminus has a strong role to play in determining the state of the salt bridge. Here, we follow the fate of the salt bridge in separate preparations of Aβ_{40} incubated with curcumin and Zn^{2+}, respectively, using solid-state nuclear magnetic resonance (ssNMR) tools. In addition, we follow the size of the soluble aggregates (with fluorescence correlation spectroscopy, FCS), the mesoscale morphology of the aggregates (with transmission electron microscopy, TEM), and the toxicity of Aβ_{40}. We then compare these results with those reported for Aβ_{42}. We draw three important inferences from our results: first, the interaction of curcumin with the C-terminal of the peptide can determine the fate of the salt bridge far away in the sequence; second, the fate of the salt bridge is associated with the toxicity of the peptide, and the mesoscale morphology of the aggregates; and third, a small molecule such as curcumin can act like a catalyst in the Aβ_{40} aggregation pathway, changing only the nature of the intermediate, but leaving the end-state nearly unaffected.

MATERIALS AND METHODS

Materials

Rink amide MBHA resin LL, Fmoc (*N*-(9-fluorenyl) methoxycarbonyl) protected amino acids, *O*-benzotriazole-*N*,*N*,*N*,*N*-tetramethyluroniumhexafluoro phosphate, and triisopropylsilane were purchased from Advanced ChemTech (Louisville, KY). 1-Hydroxybenzotriazole, *N*,*N*-dimethylformamide, collidine, TFA, *tert*-butyl methyl ether, acetonitrile, and isopropyl alcohol were obtained from S.D. Fine Chemicals (Mumbai, India). 1,8-Diazabicyclo[5.4.0] undec-7-ene, *N*-methyl morpholine, piperidine, hexafluoroisopropanol, thio-T, DMSO, 5 (6)-carboxytetramethylrhodamine *N*-succinimidyl ester, and the buffer salts are purchased from Sigma-Aldrich (St. Louis, MO). Phenol, *N*,*N*-diisopropylcarbodiimide, ethane dithiol, thioanisole, and trifluoroethanol are purchased from Fluka (Sigma-Aldrich). The isotopically labeled amino acids were purchased from Euriso-top (St. Aubin, France). All animal experimental protocols were approved by the Institute Animal Ethics committee.

Aβ_{40} sample preparation

Wild-type Aβ_{40} and three different schemes of ^{15}N-, ^{13}C-labeled Aβ_{40} were synthesized in a solid phase peptide synthesizer and further purified by a reverse-phase HPLC. The scheme 1 (*S1*) Aβ_{40} had Glu^{11}, Phe^{19}, Ala^{30}, Leu^{34}, Val^{36}, and Gly^{38} isotopically labeled with ^{15}N, ^{13}C; scheme 2 (*S2*) had Ala^{2}, Val^{12}, Phe^{20}, Asp^{23}, Ser^{26}, Lys^{28}, and Met^{35} as ^{15}N, ^{13}C labeled; and scheme (*S3*) had Asp^{23} and Lys^{28} labeled with ^{15}N, ^{13}C. Purified Aβ peptides were initially dissolved in pH 11 water (adjusted by NaOH) to prepare 2 mM stock solutions. To grow Aβ_{40} fibrils at pH 7.4, the stock solutions were diluted five times in HEPES buffer (20 mM HEPES, 146 mM sodium chloride, 5.4 mM potassium chloride, 1.8 mM $CaCl_2.2H_2O$, 0.8 mM $MgSO_4 \cdot 7H_2O$) maintained at pH 7.4 to give final peptide concentrations of 400 μM at pH 7.4. To grow Aβ_{40} fibrils in the presence of Zn^{2+} ions, the 2 mM stock solutions of Aβ_{40} were diluted five times in HEPES buffer (pH ~7.4) containing 500 μM $ZnCl_2$, giving a final solution that had 400 μM of both $ZnCl_2$ and the respective peptides. For aggregates of Aβ_{40} in the presence of curcumin, a 4 mM stock solution of curcumin was also prepared by dissolving it in pH 11.0 water. A quantity of 1.5 mL of Aβ stock (2 mM), 150 μL of freshly prepared curcumin stock (4 mM), and 7.5 μL of Rhodamine-labeled Aβ (RAβ) (100 μM) were premixed in pH 11 for 5 min, and immediately diluted with 5.85 mL HEPES buffer at pH 7.4 such that total volume was 7.5 mL. This final solution containing 400 μM Aβ, 80 μM curcumin, and 100 nM RAβ was incubated at room temperature (25°C) for four days with mild rotation (10 rpm). For making the early aggregates of Aβ_{40} in the presence of curcumin, we prepared the sample in a similar way to that described above, but with centrifugation (2700 $\times$ *g*) after 30 min of pH drop (from pH 11 to 7.4). The final pH of the solution was 7.4. The precipitate was lyophilized before packing into the NMR rotor. To grow Aβ-Cur aggregates at lower concentrations (40 μM of Aβ and 8 μM of curcumin), freshly prepared stock solutions of Aβ and curcumin (as described above) were diluted 10 times at pH 11, premixed with 7.5 μL RAβ (100 μM) for 5 min at pH 11, followed by dilution with HEPES buffer (up to 7.5 mL, pH 7.4), and incubation at room temperature (25°C) for four days with mild rotation (10 rpm).

Fluorescence correlation spectroscopy

Size of the Aβ species in solution was determined by FCS measurements following procedures similar to Sengupta et al. (31). The measurements were performed with an instrument constructed in-house (31). FCS data were fitted with a discrete component diffusion model using Origin 7.5 software (OriginLab, Northampton, MA). The diffusion times were converted to hydrodynamic radii (R_h) using rhodamine B (assumed $R_h = 0.57$ nm) as a calibrant. We used the MEMFCS (32) fitting routine developed specifically for such measurements to obtain a size distribution from the FCS data in a model-free manner.

TEM

Aβ_{40} (400 μM) and Aβ_{40}-Cur (either 400 μM Aβ_{40} + 80 μM curcumin or 40 μM Aβ_{40} + 8 μM curcumin) were aggregated for four days in HEPES buffer. Ten milliliters of these solutions were added to carbon-coated, 100-mesh copper grids (Electron Microscopy Sciences, Hatfield, PA). The extra water was blotted with tissue paper after 2–3 min, and a few mild washings were done with Milli-Q water (Millipore, Billerica, MA). A quantity of 0.1% of uranyl acetate was added for 5 min for sample staining. The grids were dried under an infrared lamp and examined in the LIBRA 120 EFTEM (Carl Zeiss, Oberkochen, Germany).

Solid-state NMR

The ssNMR measurements were performed on amyloid aggregates of Aβ_{40} peptides (400 μM) containing isotopically labeled amino acids at specific positions grown in the presence and absence of Zn^{2+} and curcumin. The aggregates were pelleted by ultracentrifugation (2700 $\times$ *g* at 20°C), washed with deionized water twice, rapidly frozen using liquid nitrogen,

and lyophilized. Powders containing Aβ_{40} peptides were packed as such without any rehydration into either 2.5, 4, or 3.2 mm magic-angle-spinning (MAS) rotors.

All the ssNMR measurements were performed in a 700 MHz model No. AVIII NMR spectrometer (Bruker, Billerica, MA) using 2.5, 3.2, or 4 mm triple-resonance MAS probes. Cross polarization from ^{1}H to ^{13}C was implemented using a linear ramped radio-frequency field (33) centered ~60–85 kHz on the ^{1}H channel and ~35–55 kHz on the ^{13}C channel depending upon the MAS frequency, ν_r (different for different experiments, as stated). Cross-polarization contact pulse time was kept between 1.5 and 4.0 ms. A swept-frequency, two-pulse phase modulation ($\phi = 10°, 15°$) decoupling scheme (34) with an ^{1}H radio-frequency field strength between 85 and 95 kHz was used to accomplish efficient ^{1}H-^{13}C dipolar decoupling. Two-dimensional (2D) ^{13}C-^{13}C through-space NMR spectra were recorded using a second-order dipolar recoupling, phase-alternated recoupling irradiation scheme (PARIS-xy) (35) with $m = 1$, $N = 2$. Mixing periods of 400 and 100 ms (ν_r = 15 kHz) were used for S^1 Aβ. For the S^2 peptide, 2D ^{13}C-^{13}C through-space correlation NMR spectra were recorded with a PARIS-xy ($m = 1$, $N = 0.5$) recoupling scheme using mixing periods of 40 and 400 ms at a ν_r of 15 kHz.

NMR data analysis

All one-dimensional (1D) spectra were processed and analyzed using the software TopSpin 2.0/3.1 (Bruker). All 2D spectra were processed with TopSpin 2.0/3.1 and analyzed using the software CCP NMR Analysis 2.2.2 (http://www.ccpn.ac.uk/homepage). The data were zero-filled in the t_1 and t_2 dimensions to 512 and 4096 points, respectively. A mixed sine/cosine ($\varphi = \pi/3$ at $t = 0$) apodization function was used in each dimension. All the spectra were externally referenced to tetramethylsilane in methanol (36).

To calculate average chemical-shift change ($\overline{\Delta\delta}$) values, ^{13}C chemical-shifts of isotopically labeled amino acids in Aβ_{40} fibrils were first subtracted from that of Aβ_{40}-Cur aggregates. These chemical-shift differences for α, β, and carbonyl carbons (the backbone), and the remaining carbons (the side chain), were then averaged over the number of carbons constituting the backbone and side chain, respectively, to obtain average chemical-shift change ($\overline{\Delta\delta}$).

Cell viability assay

The cell toxicity assay was performed on 3-day-old rat primary cortical neuronal cultures grown in 96 well plates. All the animal procedures were approved by the TIFR Animal Ethics Committee. On day 4, the primary neurons were incubated with cell culture media containing Aβ solutions (4–6 wells each at two different concentrations—first set with 400 μM Aβ_{40}, 400 μM Aβ_{40} + 80 μM curcumin, 80 μM curcumin; and second set with 40 μM Aβ_{40}, 40 μM Aβ_{40} + 8 μM curcumin, 8 μM curcumin) for 48 h. For the Zn^{2+} case, the cells were incubated in culture media containing Aβ solutions (100 μM Aβ_{40}, 100 μM Aβ_{40} + 8 μM Zn^{2+},100 μM Aβ_{42}, 100 μM Aβ_{42} + 8 μM Zn^{2+}) for 48 h. At the end of 48 h, cell media was removed and the cells were washed with Thomson's buffer at pH 7.4 (20 mM HEPES, 146 mM NaCl, 5.4 mM KCl, 2.3 mM $CaCl_2$, 0.4 mM KH_2PO_4, 0.3 mM Na_2HPO_4, 5 mM Glucose). Cells were then incubated with Thomson's buffer (pH ~7.4) containing 0.01 mg/mL propidium iodide (PI) for 10 min. PI was removed and cells were washed three times with Thomson's buffer and subsequently fixed with 4% PFA solution. The cells were then imaged for PI under an epifluorescence microscope (Axiovert 200; Carl Zeiss) using a 40× objective. The images were captured with a charge-coupled device camera (Axiocam; Carl Zeiss). Image analysis was performed for several fields in multiple dishes (at least 12 for each peptide) from three independent repeats and scored for the total number of cells (transmission images) and the number of dead cells (PI fluorescent spots). The ratio of cells that were alive (PI negative) to total cells was reported as viability. The cell viability expressed as percentage was normalized with respect to control cell viability, where the control cell viability was assumed to be 100% (actual viability in control cells was 78 ± 3%). Data are expressed as mean ± SE. Student's *t*-test was performed to test the significance of the difference of the mean number of deaths from different samples.

RESULTS

We first report the studies highlighting the effect of curcumin and Zn^{2+} on the nonstructural aspects, i.e., toxicity, aggregation kinetics, and the nature of the soluble aggregates. Structural details obtained from NMR studies are reported later.

Aβ toxicity

The effect of curcumin on Aβ_{40}-induced toxicity on rat primary cortical neuronal cultures was probed according to the protocol described in the Materials and Methods. The results of the cell viability measurement, expressed as a percentage of the control, are shown in Fig. 1 *A*. Aβ_{40} was found to be significantly toxic at a concentration of 400 μM ($p < 0.001$; Fig. 1 *Ab*). Presence of 80 μM curcumin significantly reduces the toxicity ($p < 0.001$; Fig. 1 *Ac*). However, because curcumin itself reduces the viability at such high concentrations (Fig. 1 *Ad*), the assays were also performed using 40 μM of Aβ_{40} and 8 μM of curcumin maintaining the ratio at 5:1, and still maintaining the Aβ concentration well above the saturation concentration (16 μM (37)). The toxicity of 40 μM of Aβ_{40} is lower but still substantial ($p < 0.001$; Fig. 1 *Ae*). A quantity of 8 μM of curcumin significantly reduces this toxicity ($p < 0.001$; Fig. 1 *Af*), although it is barely toxic by itself (Fig. 1 *Ag*). Similar effects on toxicity have already been reported by us in the case of Aβ_{42}, where 80 μM curcumin alleviates the toxicity induced by 400 μM of Aβ_{42} to a similar extent (21). We note that curcumin dose-response curves have been reported earlier, and concentrations in this range were found to be effective in reducing toxicity (17–19,38,39). The effect of Zn^{2+} on the toxicity of Aβ_{40} and Aβ_{42} was measured in a similar way. The concentrations of Aβ and Zn^{2+} used were 100 and 8 μM, respectively. In the case of Aβ_{40} in presence of Zn^{2+}, the viability was ~80%; in the case of Aβ_{42} ($p < 0.001$; Fig. 1 *B*), it was 50%.

Therefore, toxicity measurements do not show any qualitative difference between the effects of curcumin and Zn^{2+} on either Aβ_{40} or Aβ_{42}.

Size distribution of the soluble oligomers

FCS was used to measure the size (hydrodynamic radius) distribution of the soluble species. A quantity of 40 μM Aβ containing 100 nM of rhodamine-labeled Aβ_{40} (RhB-Aβ_{40}) was coincubated with 8 μM curcumin. FCS autocorrelation curves were measured 4 h after aggregation

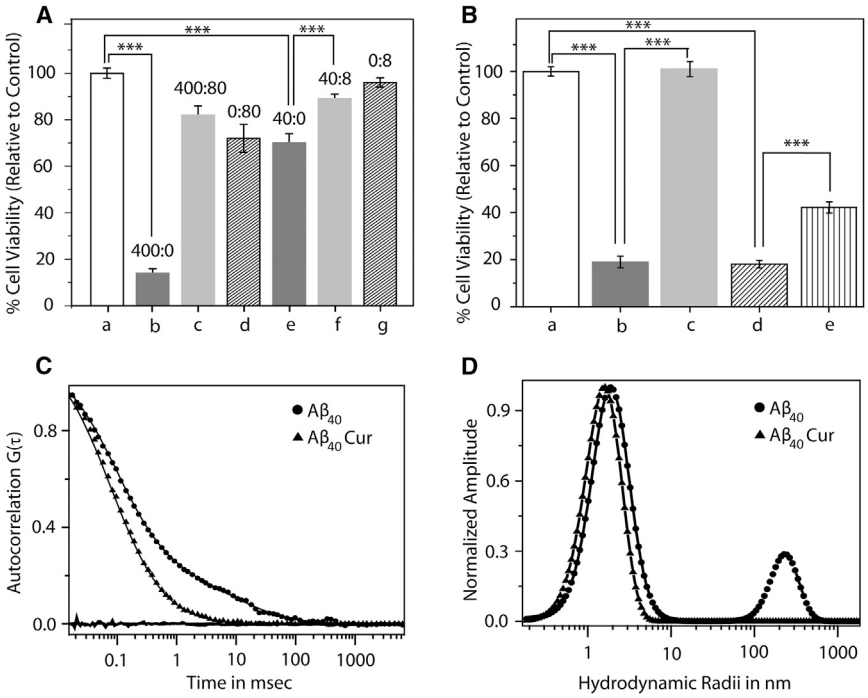

FIGURE 1 Curcumin reduces Aβ toxicity. (*A*) Cell viability assays were performed on primary cortical neurons. Cells are treated with (a) vehicle, (b) 400 μM $A\beta_{40}$, (c) 400 μM $A\beta_{40}$ and 80 μM curcumin, (d) 80 μM curcumin, (e) 40 μM $A\beta_{40}$, (f) 40 μM $A\beta_{40}$ and 8 μM curcumin, and (g) 8 μM curcumin. Percentage of live cells in vehicle (Thomson's buffer only) is normalized to 100%;***indicates that the difference is statistically significant, $p < 0.001$ (*B*) Cell viability assays performed on primary cortical neurons. Cells are treated with (a) vehicle (b) 100 μM $A\beta_{40}$ (c) 100 μM $A\beta_{40}$ and 8 μM Zn^{2+} (d) 100 μM $A\beta_{42}$ (e) 100 μM $A\beta_{42}$ and 8 μM Zn^{2+}; ***indicates that the difference is statistically significant, $p < 0.001$ (*C*) Normalized fluorescence autocorrelation data as a function of the delay time (*solid lines*) for 40 μM $A\beta_{40}$ alone (circles) and in presence of 8 μM curcumin (*triangles*). (*D*) Size distribution obtained from the MEMFCS fits presented in C (same symbols as in *C*). The abscissa is calibrated with reference to Rhodamine B. The ordinate shows the population weighted by the square of the brightness of individual particles.

was initiated with a pH drop from pH 11 to pH 7.4. The results are shown in Fig. 1, *C* and *D*. The FCS data obtained from 40 μM $A\beta_{40}$ in presence (*triangles*) and absence (*circles*) of curcumin (Fig. 1 *C*) were fitted with a quasi-continuous size distribution model using the MEMFCS fitting routine (32) (Fig. 1 *D*). Here, the abscissa represents the hydrodynamic radii in nanometer (this axis is calibrated by measuring the diffusion of rhodamine B in water, which has a hydrodynamic radius of 0.57 nm (40)), and the ordinate represents the relative population weighted by the square of the particle brightness (32). The first peak at ~2 nm corresponds to the monomeric and the small oligomeric species, while the second peak at ~200 nm corresponds to the larger, quasi-stable, soluble aggregates. We observe that the large soluble aggregates are no longer detectable when curcumin is present in the solution (Fig. 1 *D*), implying that curcumin accelerates the precipitation of these aggregates and they grow in the precipitate phase. We also observe a small shift and a narrowing of the first peak, which indicate a simultaneous decrease of the population of smaller oligomers.

We have previously shown that Zn^{2+} also rapidly precipitates the soluble aggregates of $A\beta_{40}$ and $A\beta_{42}$ (23), indicating that both curcumin and Zn^{2+} have similar effects on both the peptides.

TEM measurements of the fibrils

TEM images of $A\beta_{40}$ and $A\beta_{42}$ were recorded at two different peptide/curcumin concentrations: 40 μM (Fig. 2 *B* for $A\beta_{40}$; Fig. 2 *E* for $A\beta_{42}$) and 400:80 μM (Fig. 2 *C* for $A\beta_{40}$; Fig. 2 *F* for $A\beta_{42}$). The $A\beta_{40}$ aggregates grown in the presence of curcumin do form fibril-like structures, in some cases growing beyond 100 nm (marked by *solid rectangles* in Fig. 2). However, they are much shorter than the fibrils grown without curcumin. In contrast, the aggregates of curcumin-incubated $A\beta_{42}$ are shorter and more disordered (Fig. 2, *E* and *F*), consistent with what we have previously reported (21). A measurement of the length distribution of the aggregates of $A\beta_{40}$ versus $A\beta_{42}$ quantitatively shows that the average length of the fibrils is indeed much larger for $A\beta_{40}$ (Fig. S1). We have earlier shown that Zn^{2+} completely disrupts fibril formation (29). In summary, while both curcumin and Zn^{2+} disrupt fibrilization of both the Aβ peptides, curcumin-incubated $A\beta_{40}$ shows less disruption than others.

Atomic-level contacts probed by solid-state NMR

We then probed the atomic-level structural changes in $A\beta_{40}$ aggregates induced by Zn^{2+} and curcumin, respectively, using ssNMR. We designed two different ^{13}C and ^{15}N labeled amino-acid schemes to monitor different regions of the peptide including the turn, the tail, and the two hydrophobic arms. Scheme 1 (*S1*) covers mainly the hydrophobic arms and has Glu^{11}, Phe^{19}, Ala^{30}, Leu^{34}, Val^{36}, and Gly^{38} isotopically labeled. Scheme 2 (*S2*) includes mainly the turn (including the salt-bridge forming residues) and tail regions and has Ala^{2}, Val^{12}, Phe^{20}, Asp^{23}, Ser^{26}, Lys^{28}, and Met^{35} isotopically labeled. We performed separate ssNMR

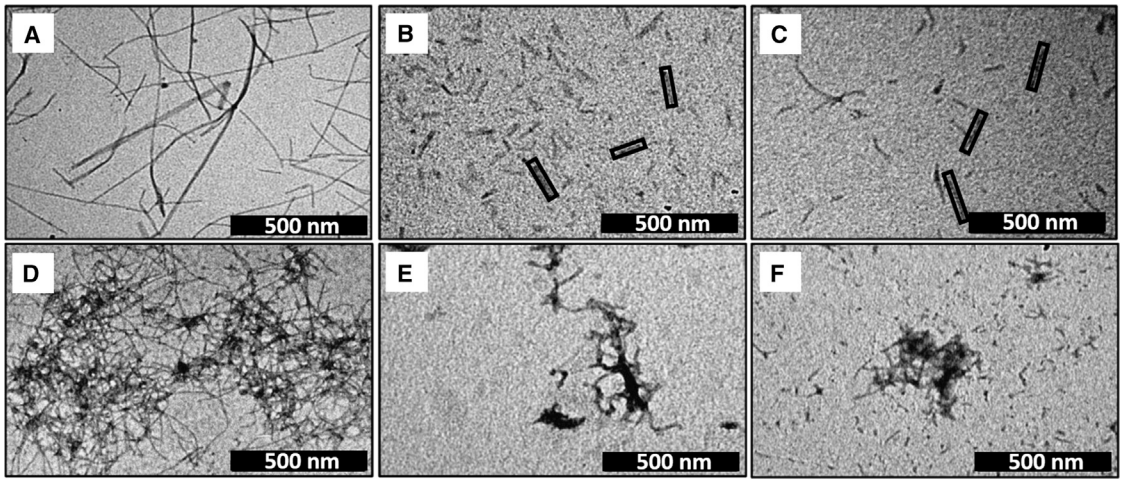

FIGURE 2 TEM images of amyloid aggregates. (*A*) 400 μM Aβ_{40}, (*B*) 40 μM Aβ_{40} grown in the presence of 8 μM curcumin, and (*C*) 400 μM Aβ_{40} grown in the presence of 80 μM curcumin. (*Solid rectangles*) Short fibrillar structures are shown. (*D*) 400 μM Aβ_{42}, (*E*) 40 μM Aβ_{42} were grown in the presence of 8 μM curcumin, and (*F*) 400 μM Aβ_{42} were grown in the presence of 80 μM curcumin. Scale bars, 500 nm.

measurements on specimens incubated in curcumin for 30 min and four days. We focused on the two distal interresidue contacts established in the mature fibrils of Aβ_{40}, namely, the contact between F19 and L34, and the salt-bridge contact between D23 and K28. It is known that the F19–L34 contact is already established in the early oligomers, but the salt-bridge region appears different in this species (1). Fig. 3 *A* shows an overlay of 2D ^{13}C-^{13}C PARIS-xy ($m = 1$, $N = 2$) spectra of Aβ_{40} (*black* online) and Aβ_{40}-Cur (incubated for four days; *red* online) aggregates of scheme *S1* recorded with 400 ms of mixing time. Fig. 3 *B* shows the same for Aβ_{40} (*scheme S1*) incubated with Zn^{2+}. These spectra do not exhibit any drastic changes in peak positions or intensities compared to the spectra obtained from Aβ alone. The presence of the cross peak, indicating the spatial contact between aromatic carbons ($\delta/\varepsilon/\zeta$) of Phe^{19} and side-chain carbons (γ/δ) of Leu^{34} (highlighted with *dotted square*), suggests that the hairpin shape remains largely unperturbed. However, the cross-peak intensity in the case of Aβ_{40}-Zn^{2+} aggregates is weaker than that in the Aβ_{40}-Cur aggregates. For Aβ_{42}-Zn^{2+} and Aβ_{42}-Cur, the cross-peak intensities largely remain similar to the wild-type Aβ_{42} (21,29). Overall, curcumin and Zn^{2+} do not strongly perturb the core hydrophobic region of either of the peptide variants.

We then probed the changes induced by Zn^{2+} on the sample Scheme 2 (*S2*). Fig. 4 *A* shows an overlay of 2D ^{13}C-^{13}C PARIS-xy ($m = 1$, $N = 0.5$) spectra of Aβ_{40} (*black* online) and Aβ_{40}-Zn^{2+} (*red* online) aggregates. Even though the two spectra in Fig. 4 *A* appear similar, significant changes in the nature (pertaining to conformational changes), chemical shift, as well as the intensity of cross peaks corresponding to amino acids Asp^{23} and Lys^{28}, are observed. Cross peaks belonging to Lys^{28} are not only shifted, but are also considerably weaker. For the wild-type Aβ_{40}, in the ^{13}C 1D spectrum, Asp^{23} shows two peaks at 178.1 ppm and at 180.1 ppm. Similarly N_ζ of Lys^{28} shows two peaks at 38.2 and 34 ppm. A frequency-selective REDOR experiment was performed to confirm that the C_γ peak of Asp^{23} at 180.1 ppm forms a salt bridge with N_ζ of Lys^{28} (Fig. 5 *D*). Fig. 4 *B* shows the 1D sum projection extracted from the 2D ^{13}C-^{13}C spectra in the carbonyl region of Aβ_{40}-Zn^{2+}. In the case of fibrils grown in the presence of Zn^{2+}, the peak corresponding to the salt-bridge-forming carbonyl group (~180 ppm) of the side chain of Asp^{23} is replaced by a broad peak (~178 ppm) (29). Also, the ^{15}N 1D spectra in Fig. 4 *C*, shows a change in the chemical shift from 38.2 ppm (fibril) to 34 ppm (fibril-Zn^{2+}). This redistribution of Asp^{23} and Lys^{28} population for Aβ_{40}–Zn^{2+} is very similar to what was observed for Aβ_{42}-Zn^{2+} previously (29). REDOR experiments showed that for Aβ_{42}-Zn^{2+}, the ~178 ppm peak corresponds to a non-salt-bridge-forming species. The broad envelope of Asp^{23} C_γ peak (~178 ppm) in Aβ_{40}-Zn^{2+} prevented us from performing REDOR experiments. However, as the chemical shift pattern of Asp^{23} and Lys^{28} for Aβ_{40}-Zn^{2+} is very similar to that of Aβ_{42}-Zn^{2+}, we infer that Aβ_{40}-Zn^{2+} also does not have the salt bridge. Based on the chemical shift value, the non-salt-bridge-forming Lys^{28} side-chain N_ζ seems to be uncharged (41), which would indicate a local pKa change for the side chain of Lys^{28}. However, additional experiments will be required to determine the charge state of N_ζ. Fig. 4, *D* and *E*, shows an overlay of Aβ_{40} (*solid*), Aβ_{40}-Zn (*shaded*), and Aβ_{40} small oligomer spectra (adapted from Sarkar et al. (1); *dark dotted shading*). This highlights the peaks belonging to the salt-bridge-forming Asp^{23} side chain. The conformations of Asp^{23} and Lys^{28} are very similar in the small oligomers and in the Zn^{2+} captured Aβ_{40}, suggesting that Zn^{2+} captures the salt-bridge region in the oligomeric state, and arrests any further development of this region even as aggregation proceeds. Aβ_{42}-Zn^{2+} aggregates also showed a very similar result (29).

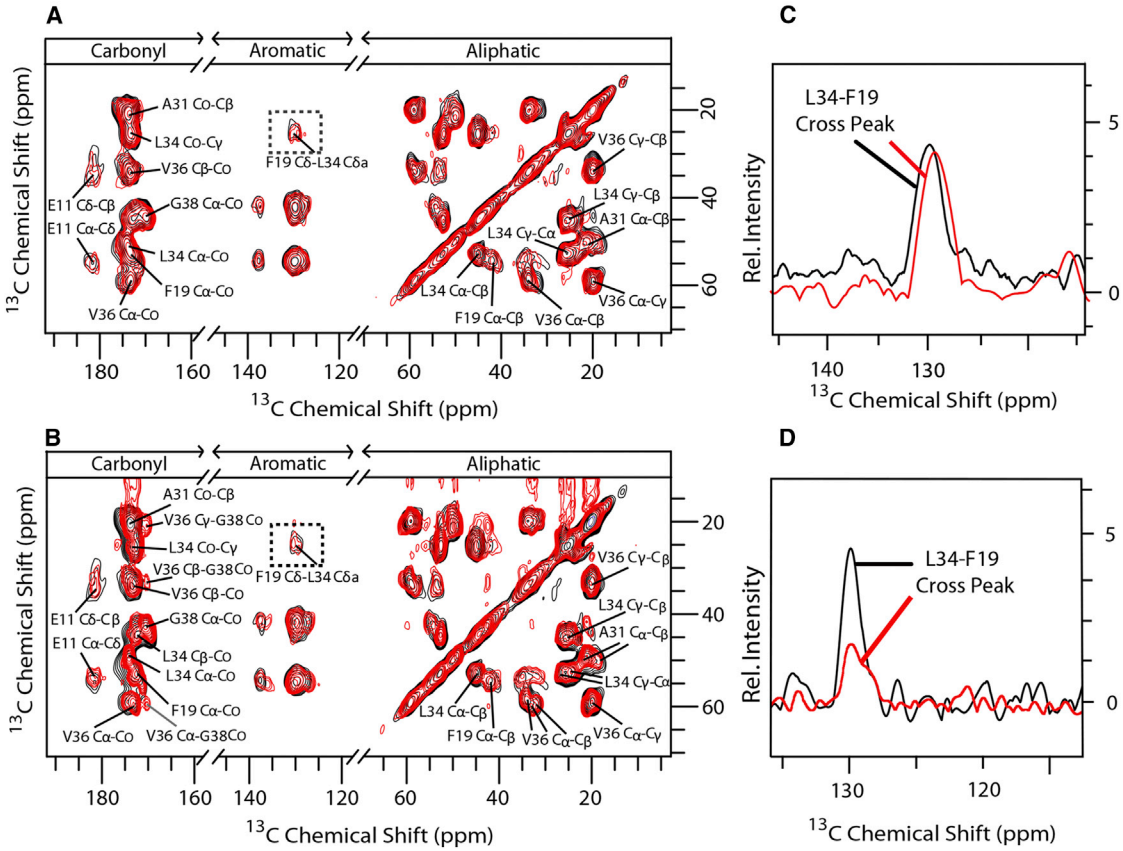

FIGURE 3 Effect of Zn^{2+} and curcumin on the hydrophobic region of Aβ. (*A*) Shown here is an overlay of 2D ^{13}C-^{13}C PARIS-xy ($m = 1, N = 2$) spectra of Aβ_{40} (*black* online) and Aβ_{40}-Cur (*red* online) aggregates of isotopic labeling scheme 1 recorded with a mixing time of 400 ms. (*Dotted rectangles*) Cross peaks between aromatic carbons of Phe^{19} and side-chain γ/δ carbons of Leu^{34} are shown, and (*B*) corresponding spectra with Zn^{2+}. (*C*) The cross peaks highlighted in (*A*) extracted as a sum projection of rows between 20.5 and 27 ppm from the 2D spectrum of Aβ_{40} (*black* online) and Aβ_{40}-Cur aggregates (*red* online) are depicted, with (*D*) a similar sum projection for Zn^{2+} aggregates. To see this figure in color, go online.

Fig. 5 *A* shows an overlay of 2D ^{13}C-^{13}C PARIS-xy ($m = 1$, $N = 0.5$) spectra of Aβ_{40} (*black* online) and Aβ_{40}-Cur (*red* online) aggregates (four days old) recorded from isotopic labeling scheme 2 (*S2*) with a mixing time of 40 ms. The Asp^{23} and Lys^{28} cross peaks overlap with each other. Fig. 5, *B* and *C*, shows overlay of ^{13}C 1D spectra of the carbonyl region and ^{15}N 1D spectrum, respectively, of Aβ_{40} (*black* online) and Aβ_{40}-Cur (*red* online) aggregates. The δ-carbon of Asp^{23} shows a major peak at 180.5 ppm and a minor peak at 179 ppm (Fig. 5 *B*). ζ-Nitrogen of Lys^{28} gives rise to two maxima at 36.2 and 38.3 ppm in Aβ_{40} aggregates, and similar peaks for Aβ_{40}-Cur aggregates as well (Fig. 5 *C*). Salt-bridge formation was further probed by fs-REDOR measurements between γ-carbon of Asp^{23} and ζ-nitrogen of Lys^{28}, the results of which are shown in Fig. 5 *D*. For an isolated ^{13}C-^{15}N pair, the S_1/S_0 value is expected to reach one-half of its initial value at $\tau_{mix} = 0.257$ ms $\times$ $(R_{NC}/\text{Å})^3$, where τ_{mix} is the REDOR dephasing time, and R_{NC} is the internuclear distance (28,42). REDOR dephasing curves of Asp^{23} in both Aβ_{40} and Aβ_{40}-Cur aggregates yielded a half-maximum ($S/2S_0$) between 17.1 and 21.2 ms, corresponding to a ^{13}C-^{15}N distance of 4.0–4.4 Å. This shows that Asp^{23} in both cases forms a salt bridge with Lys^{28}. The presence of the salt bridge in Aβ_{40}-Cur aggregates distinguishes it from Aβ_{42}-Cur (21), and also from Aβ_{42}-Zn (29) and Aβ_{40}-Zn aggregates.

We then tested if the changes observed at four days are present from the early stages of aggregation. We separately recorded 2D ^{13}C-^{13}C correlation spectra from the early aggregates (30 min) of Aβ_{40}, in the presence of curcumin (Fig. 5 *E*). We observe that the peak corresponding to the salt-bridge conformation of Asp^{23} (~180.4 ppm) is missing at 30 min. Fig. 5 *E* shows significant similarity in spectra yielded by these 30-min-old Aβ_{40}-Cur aggregates and the small oligomers of pure Aβ_{40} (shown in *dotted blue* online) (1), showing that initial interaction of curcumin with the small oligomers of Aβ_{40} is similar to that of Zn^{2+}.

Fig. 6 shows changes in chemical shifts in the α, β, and carbonyl carbons of all conformations of labeled amino acids in Aβ_{40}, when aggregated in the presence of Zn^{2+} (Fig. 6 *A*) and curcumin (Fig. 6 *B*). The secondary chemical shift data show that in Aβ_{40}-Zn^{2+} aggregates, the β-sheet extends to 1–2 more residues compared to Aβ_{40}. At the C-terminal, many of the amino acids seem to have

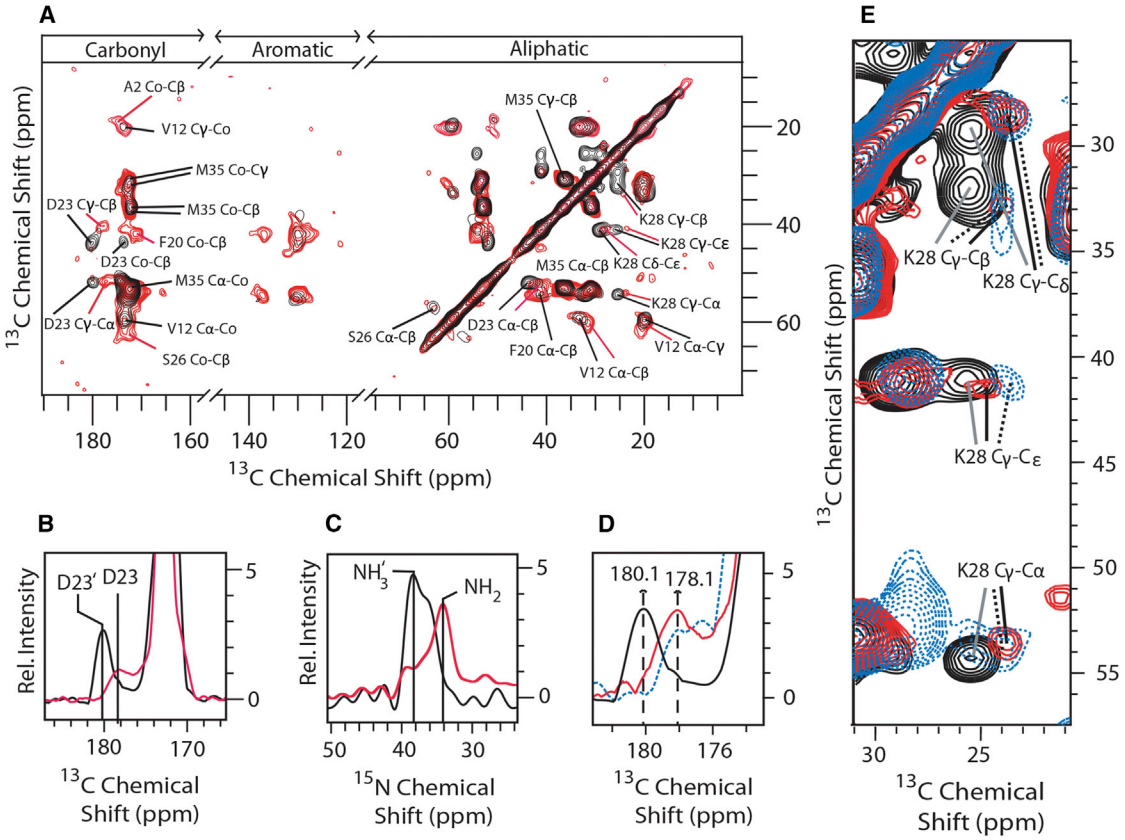

FIGURE 4 Effect of Zn^{2+} on the turn region and the salt bridge of Aβ. (*A*) Overlay of 2D ^{13}C-^{13}C PARIS-xy ($m = 1, N = 0.5$) spectrum of Aβ_{40} (*black* online) and Aβ_{40}-Zn^{2+} (*red* online) aggregates of isotopic labeling scheme 2 recorded with a mixing time of 100 ms. (*B*) Selected region of the ^{13}C 1D slice of Aβ_{40} fibril (*black* online) overlapped on that of Aβ_{40}-Zn^{2+} (*red* online). (*C*) Selected region of the ^{15}N 1D spectrum of Aβ_{40} fibril (*black* online) overlapped on that of Aβ_{40}-Zn^{2+} (*red* online). (*D*) 1D sum projections of rows between 35 and 56.4 ppm extracted from 2D ^{13}C-^{13}C spectra of Aβ_{40} fibrils (*black* online), Aβ_{40}-Zn^{2+} aggregates (*red* online) and Aβ_{40} small oligomers (*dotted blue* online, shown in *E*). (*E*) A selected region of 2D ^{13}C-^{13}C PARIS-xy ($m = 1, N = 0.5$) spectrum of Aβ_{40} fibrils (*black* online) overlaid on that of Aβ_{40}-Zn^{2+} aggregates (*red* online) and Aβ_{40} small oligomers (*dotted blue* online). To see this figure in color, go online.

unchanged conformation in Aβ_{40}-Zn^{2+}, such as V36, M35, A30, and G38. However, there is more structural heterogeneity in the N-terminal region, as indicated by the multiple peaks observed for A2. E11 and V12, which also show stronger and more heterogeneous cross peaks compared to the Aβ_{40} fibrils. In Aβ_{40} fibrils the N-terminal β-sheet region starts from the E11 residue and extends up to D23, whereas, in Aβ_{40}-Zn^{2+}, E11 and V12 have one of the conformations in a non-β-sheet state (Fig. S2). A clear C_β-CO cross peak of F20 in Aβ_{40}-Zn^{2+} (Fig. 4 *A*) suggests a more rigid conformation in the surrounding region, compared to Aβ_{40} alone. In all the cases, the main difference arises due to changes in the chemical shift of the carbonyl carbon. Aβ_{42}-Zn^{2+} aggregates did not show any chemical shift change or population redistributions (except for D23, K28, and S26 residues) (29).

Aβ_{40}-Cur aggregates do not show any strong differences at the N-terminal in comparison with Aβ_{40}. There is a small chemical shift difference for A2, and for V12 (Fig. 5 *A*). In both, the β-sheet starts forming E11 on the N-terminal (Fig. S2). The backbone of E11, V12, and side chain of V12 and F19 undergo structural changes in the presence of curcumin. As observed in the case of Aβ_{42}, curcumin has an effect on the chemical shift of V12 and E11 (21). In the C-terminal, the effect of curcumin on V36 is similar in both Aβ_{42} (21) and Aβ_{40}, with curcumin causing population redistribution among two conformers of V36 leading to the total disappearance of V36′. However, unlike Aβ_{42}-Cur (21), we did not see curcumin causing any changes in the spectra of L34 and G38 in Aβ_{40}.

Fig. 6, *C* and *D*, summarizes the structural elements in Aβ_{40} that appear to interact with Zn^{2+} and curcumin, respectively. All amino acids labeled with ^{13}C and ^{15}N are marked with double circles. Amino acids that participate in a significant structural change, i.e., those suffering a chemical-shift change of $\overline{\Delta\delta} \geq 0.5$ ppm, are highlighted in filled light blue online. Amino acids showing changes in relative population among different structural conformers are highlighted with a dotted red online. Filled green online Asp^{23} and Lys^{28} that undergo a structural change only in the early oligomers, but not in the mature aggregates. The full table of chemical shifts is provided in Table S1.

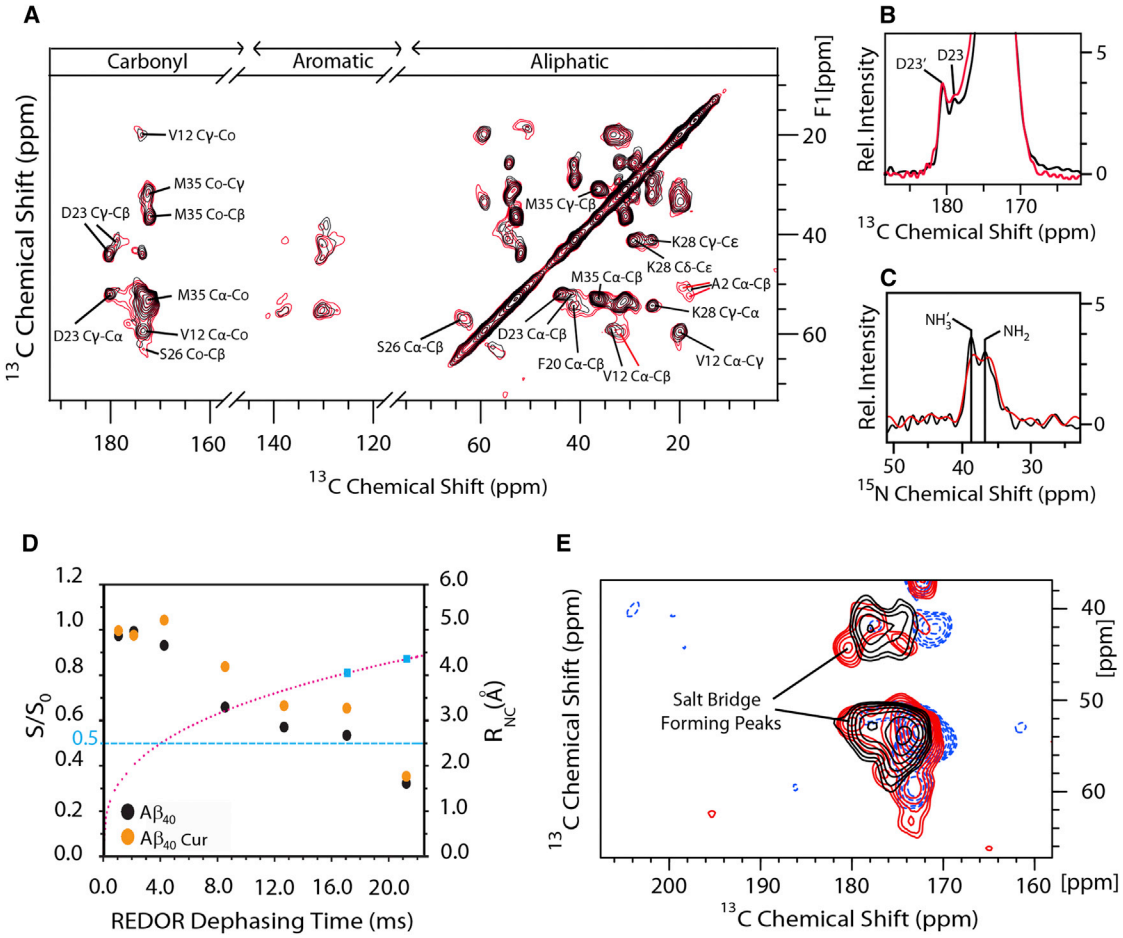

FIGURE 5 Effect of curcumin on the turn region of Aβ. (*A*) Shown here is an overlay of 2D ^{13}C-^{13}C PARIS-xy ($m = 1, N = 0.5$) spectra of Aβ_{40} (*black* online) and Aβ_{40}-Cur (*red* online) aggregates of isotopic labeling scheme 2 recorded with a mixing time of 40 ms. (*B*) Here is an overlay of 1D ^{13}C spectrum of Aβ_{40} (*black* online) and Aβ_{40}-Cur (*red* online) showing peaks of two conformations of the δ-carbon of Asp^{23}, as indicated. (*C*) Shown here is an overlay of 1D ^{15}N spectrum of Aβ_{40} (*black* online) and Aβ_{40}-Cur (*red* online) showing two conformations of amide ζ-nitrogen of Lys^{28}. (*D*) Here, we probe salt-bridge formation between Asp^{23} and Lys^{23} with fs-REDOR. Dephasing curves for Aβ_{40} and Aβ_{40}-Cur aggregates, obtained by monitoring the peak height of the γ-carbon in Asp^{23} with (S) and without (S_0) ^{13}C-^{15}N dipolar recoupling, are shown. (*Dotted line*) Here is variation of R_{NC} as a function of τ_{mix}. (*Solid squares on top of the dotted line*) R_{NC} values of 4.0 and 4.4 Å corresponding to τ_{mix} values of 17.1 and 21.2 ms are given. (*E*) Shown here is an overlay of 2D ^{13}C-^{13}C PARIS-xy ($m = 1, N = 0.5$) spectra of 4-day-old aggregates of Aβ_{40}-Cur (*red* online; scheme 2) and 30-min aggregates of Aβ_{40} grown in the presence of curcumin in HEPES buffer (*black* online; scheme 3), and Aβ_{40} small oligomers (*dotted blue* online; scheme 2; sample preparation mentioned in (1)) recorded with a mixing time of 40 ms. (*Solid arrow*) The salt-bridge-forming peaks at 180.1 ppm are missing in 30-min aggregates and small oligomers. To see this figure in color, go online.

DISCUSSION

In this work we investigate the structural correlates of Aβ toxicity reduction caused by Zn^{2+} and curcumin, focusing on the central salt bridge observed in Aβ fibrils. Further, we compare these results for both Aβ_{40} and Aβ_{42}, to probe the conformational connection between the C-terminal and the central salt bridge. We first establish the reduction of toxicity of the Aβ species on which we performed the experiments. We then measure the stability of the soluble oligomers, and the morphology of the mature aggregates, and investigate the atomic level changes in the structure of the hydrophobic core and of the salt-bridge regions of the peptide. As we discuss below, these results lead to a consistent picture of the connection among the state of the salt bridge, the fibril morphology, and toxicity. Most importantly, we find that interactions at the C-terminus can alter the state of the salt bridge, located far away in the sequence, and also in physical distance according to most of the structural models (21,29).

Reduction of toxicity is likely due to the precipitation of the oligomeric species

FCS measurements described in Fig. 1 suggest that a major effect of curcumin is to precipitate the soluble aggregates of Aβ. While the large soluble aggregates (~200 nm) are completely precipitated by curcumin, even the smaller aggregates are affected. Similar observations were made by

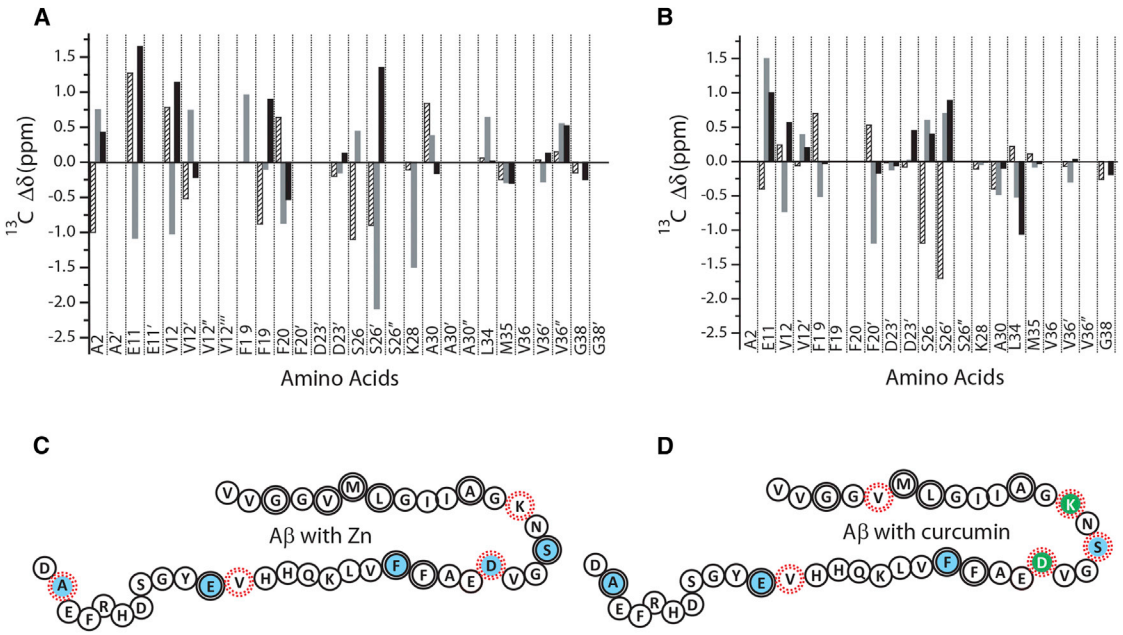

FIGURE 6 Changes in the chemical-shift and conformations of Aβ in the presence of Zn^{2+} and curcumin. The chemical-shift difference between Aβ_{40} and Aβ_{40}-Zn^{2+} aggregates (*A*), and Aβ_{40} and Aβ_{40}-Cur aggregates (*B*) for α (*hatched bars*), β (*shaded bars*), and carbonyl (*solid bars*) carbons. The vacant places define extra conformation of one species, which is missing on the other. Amino acids showing structural changes in the presence of Zn^{2+} (*C*), and curcumin (*D*), are highlighted in the schematic hairpin model of Aβ_{40} where each circle represents a particular amino acid. All amino acids labeled with ^{13}C and ^{15}N are marked with double-circle boundaries. Amino acids incurring a significant structural change, i.e., the ones that cause chemical-shift changes $\overline{\Delta\delta} \geq 0.5$ ppm, are highlighted with filled light blue online. Amino acids showing population changes among their different structural conformers are highlighted with dotted red online. Filled green online highlights Asp^{23} and Lys^{28}, which undergo a structural change only in the early oligomers, but not in the mature aggregates. To see this figure in color, go online.

us (23) when we incubated 8 μM Zn^{2+} with 10 and 20 μM Aβ_{40} (23). Reports suggest that the soluble aggregation intermediates, and not the final mature fibrils, are responsible for Aβ toxicity (43–45). Therefore, the sequestration of these species by curcumin and Zn^{2+} is likely the key cause of the reduction of toxicity. We note that our results cannot distinguish which of the aggregation intermediates is the most toxic, because both curcumin and Zn^{2+} precipitate a large range of aggregates.

Curcumin allows ordered fibril formation

It is known that Zn^{2+} strongly disrupts fibril formation for both Aβ_{42} and Aβ_{40} (23,46). Because Zn^{2+} preferentially interacts near the N-terminus (i.e., with histidine residues 6, 13, and 14), it suggests that this region has a strong role to play in determining the state of the salt bridge, located far away both in sequence and in space (29). On the other hand, Fig. 2 shows that while curcumin shortens the length of Aβ_{40} fibrils, it does not stop fibril formation altogether. Significantly, it disrupts or reduces the fibril length more in Aβ_{42} than in Aβ_{40} (Fig. 2, *E* and *F*). Because its major site of interaction with Aβ is at the C-terminal (21), it indicates that the conformation of the C-terminal can also strongly affect the morphology of the fibrils (21,29), and a putative weakening of this interaction in Aβ_{40} (due to the missing hydrophobic residues I41 and A42) also weakens this effect.

Oligomers retain their hairpin conformation with both curcumin and Zn^{2+}

Oligomers are characterized by a distal contact formed between F19 and L34, which is retained in the fibril. The row projection of the ssNMR spectra shows the F19-L34 cross peak in Aβ_{40} incubated with either curcumin (Fig. 3 *C*) or Zn^{2+} (Fig. 3 *D*), indicating that the tertiary fold is maintained in the presence of both the reagents. Similar observations were made in the case of Aβ_{42} earlier (21,29). However, for Aβ_{40} the cross peaks become relatively weak in aggregates grown in the presence of Zn^{2+}, indicating some distortions of the hairpin fold.

Oligomers are arrested in their non-salt-bridged state by Zn^{2+}

ssNMR observations reported here indicate that the salt bridge between Lys^{28} and Asp^{23} is at least partially disrupted in the Zn^{2+}-incubated fibrils of Aβ_{40} (Fig. 4). Noy et al. (46) have predicted a possible structural perturbation of Aβ_{40} in the salt-bridge region by Zn^{2+}, but the status of the salt bridge was not clear in their study. We have reported

before that the salt bridge is absent in the Zn^{2+} incubated fibrils of Aβ_{42} (29). While this was interpreted as Zn^{2+} breaking the salt bridge (29), it is possible that Zn^{2+} simply captures Aβ_{42} in an oligomeric state that is yet to evolve a stable salt bridge, and keeps it that way. We note that the presence or absence of the salt bridge in the oligomeric form is not yet established for Aβ_{42}. Moreover, recent reports suggest that the terminal A42 and not D23 may form the salt bridge with K28 (8,9). However, in Aβ_{42} containing a C-terminal amide (our preparation), the salt bridge is clearly formed between D23 and K28 (29). This indicates that different fibrillar polymorphs of the natural peptide probably exist, and small changes in the C-terminal may cause large changes in the nature of the salt bridge.

Curcumin allows the salt bridge to form in Aβ_{40}

Our results show that the salt bridge is present in the curcumin-incubated fibrils of Aβ_{40} (Fig. 5). This gives rise to two possibilities: either curcumin induces immediate salt-bridge formation in the oligomers, or it allows salt-bridge formation at a later stage, when the fibrils form. To decide between these possibilities, we looked at the Aβ aggregates precipitated by curcumin at an early stage (30 min). We found that the salt-bridge-forming peaks of Asp^{23} are absent at this stage (Fig. 5 *E*), indicating that curcumin allows salt-bridge formation only at a later stage. However, for Aβ_{42}, curcumin does not allow formation of the salt bridge or of well-ordered fibrils even in the later stage.

It is interesting to speculate why curcumin allows Aβ_{40} to form the salt bridge at a later stage of growth. We have found earlier that curcumin interacts strongly with the 34th, 36th, and 38th residues on the C-terminal of Aβ_{42} (21). However, here we do not observe any substantial change induced by curcumin in L34 and G38 of Aβ_{40}. This indicates that interaction of Aβ_{40} with curcumin is much weaker than that with Aβ_{42}. Two additional hydrophobic residues (I41 and A42) on the C-terminal thus seem to play a crucial role in the way Aβ interacts with curcumin. It is likely that a stronger interaction of curcumin with these extra two amino acids in Aβ_{42} prevents the formation of the salt bridge, but a weaker restriction imposed on the Aβ_{40} molecules allows the aggregation to proceed such that the peptide ultimately forms the salt bridge. We note that it is possible that curcumin has a much lower affinity for the mature aggregates of Aβ_{40}, and may tend to dissociate from them as the aggregates mature. In contrast, Zn^{2+} likely interacts with the histidine-containing N-terminal region of Aβ (25–27), which is identical in sequence in both Aβ_{40} and Aβ_{42}, and consequently has the same effect on both.

Significantly, the fibril morphology seems to be correlated with the presence of the salt bridge. Zn^{2+}-incubated samples never form regular fibrils (23,46), while curcumin-incubated ones do form fibril-like features, though of a shorter length (Fig. 2). It has also been shown by others recently that Aβ_{40} is able to form fibrils in the presence of curcumin (18). There are also reports on other phenolic compounds that can interact with Aβ_{40} in the C-terminal, and still allow salt-bridge formation between D23 and K28 (47).

CONCLUSIONS

We conclude that both Zn^{2+} and curcumin reduce Aβ toxicity by precipitating the non-salt-bridged oligomers. However, curcumin eventually allows the formation of the salt bridge in Aβ_{40}, likely due to its weaker C-terminal-mediated interaction with the peptide. This shows the strong effect of the C-terminal residues on the D23-K28 salt bridge, which is far removed from it in the sequence. The effects of Zn^{2+} indicate that the N-terminal also can have a similar effect on the central salt bridge. Thus the N-terminal, the C-terminal, and the central salt bridge containing regions of Aβ appear to have a clear conformational link. This helps to explain several known facts about Aβ toxicity. First, this conformational link suggests that Aβ_{42} can be more toxic than the shorter Aβ_{40} by differently controlling the salt-bridge region, which possibly plays a major role in determining the toxicity of these peptides. It also suggests that most of the mutations leading to early onset AD may actually reflect different facets of a unified toxicity mechanism. In addition, it appears that curcumin preferentially interacts with Aβ_{40} aggregation intermediates, and changes their toxicity—but does not strongly interact with the mature end-product of aggregation. Thus, curcumin can be a starting point for developing a catalytic agent that can modulate the aggregation pathway, reducing toxicity without a net thermodynamic cost.

SUPPORTING MATERIAL

Two figures and one table are available at http://www.biophysj.org/biophysj/supplemental/S0006-3495(17)30287-4.

AUTHOR CONTRIBUTIONS

S.M. and P.K.M. designed and conceptualized the experiments. B.C. and V.S.M. performed the NMR experiments and analyzed the data. D.B. performed and analyzed the TEM. A.K.D. performed the cell toxicity studies. B.S. performed the FCS studies. S.M., P.K.M., B.C., and V.S.M. cowrote the article. All authors discussed the results and commented on the article.

ACKNOWLEDGMENTS

We acknowledge the National Facility for High-Field NMR and Manoj Naik for assistance in NMR experiments, and the Cryo-TEM facility and Lalit Borde for help with the TEM measurements.

B.C. acknowledges a CSIR-SPM-SRF fellowship.

REFERENCES

1. Sarkar, B., V. S. Mithu, …, S. Maiti. 2014. Significant structural differences between transient amyloid-β oligomers and less-toxic fibrils in regions known to harbor familial Alzheimer's mutations. *Angew. Chem. Int. Ed. Engl.* 53:6888–6892.
2. Bucciantini, M., E. Giannoni, …, M. Stefani. 2002. Inherent toxicity of aggregates implies a common mechanism for protein misfolding diseases. *Nature.* 416:507–511.
3. Chiti, F., and C. M. Dobson. 2006. Protein misfolding, functional amyloid, and human disease. *Annu. Rev. Biochem.* 75:333–366.
4. Sevigny, J., P. Chiao, …, A. Sandrock. 2016. The antibody aducanumab reduces Aβ plaques in Alzheimer's disease. *Nature.* 537:50–56.
5. Lu, J. X., W. Qiang, …, R. Tycko. 2013. Molecular structure of β-amyloid fibrils in Alzheimer's disease brain tissue. *Cell.* 154:1257–1268.
6. Petkova, A. T., Y. Ishii, …, R. Tycko. 2002. A structural model for Alzheimer's β-amyloid fibrils based on experimental constraints from solid state NMR. *Proc. Natl. Acad. Sci. USA.* 99:16742–16747.
7. Xiao, Y., B. Ma, …, Y. Ishii. 2015. Aβ(1–42) fibril structure illuminates self-recognition and replication of amyloid in Alzheimer's disease. *Nat. Struct. Mol. Biol.* 22:499–505.
8. Colvin, M. T., R. Silvers, …, R. G. Griffin. 2016. Atomic resolution structure of monomorphic Aβ42 amyloid fibrils. *J. Am. Chem. Soc.* 138:9663–9674.
9. Wälti, M. A., F. Ravotti, …, R. Riek. 2016. Atomic-resolution structure of a disease-relevant Aβ(1–42) amyloid fibril. *Proc. Natl. Acad. Sci. USA.* 113:E4976–E4984.
10. Klein, A. M., N. W. Kowall, and R. J. Ferrante. 1999. Neurotoxicity and oxidative damage of β-amyloid 1–42 versus β-amyloid 1–40 in the mouse cerebral cortex. *Ann. N. Y. Acad. Sci.* 893:314–320.
11. Cruts, M., J. Theuns, and C. Van Broeckhoven. 2012. Locus-specific mutation databases for neurodegenerative brain diseases. *Hum. Mutat.* 33:1340–1344.
12. Chong, S. H., J. Yim, and S. Ham. 2013. Structural heterogeneity in familial Alzheimer's disease mutants of amyloid-β peptides. *Mol. Biosyst.* 9:997–1003.
13. Weggen, S., and D. Beher. 2012. Molecular consequences of amyloid precursor protein and presenilin mutations causing autosomal-dominant Alzheimer's disease. *Alzheimers Res. Ther.* 4:9.
14. Reinke, A. A., and J. E. Gestwicki. 2007. Structure-activity relationships of amyloid β-aggregation inhibitors based on curcumin: influence of linker length and flexibility. *Chem. Biol. Drug Des.* 70:206–215.
15. Hamaguchi, T., K. Ono, and M. Yamada. 2010. REVIEW: Curcumin and Alzheimer's disease. *CNS Neurosci. Ther.* 16:285–297.
16. Garcia-Alloza, M., L. A. Borrelli, …, B. J. Bacskai. 2007. Curcumin labels amyloid pathology in vivo, disrupts existing plaques, and partially restores distorted neurites in an Alzheimer mouse model. *J. Neurochem.* 102:1095–1104.
17. Yang, F., G. P. Lim, …, G. M. Cole. 2005. Curcumin inhibits formation of amyloid β-oligomers and fibrils, binds plaques, and reduces amyloid in vivo. *J. Biol. Chem.* 280:5892–5901.
18. Thapa, A., S. D. Jett, and E. Y. Chi. 2016. Curcumin attenuates amyloid-β aggregate toxicity and modulates amyloid-β aggregation pathway. *ACS Chem. Neurosci.* 7:56–68.
19. Sun, Q., N. Jia, …, H. Hu. 2014. Activation of SIRT1 by curcumin blocks the neurotoxicity of amyloid-β25–35 in rat cortical neurons. *Biochem. Biophys. Res. Commun.* 448:89–94.
20. Mutsuga, M., J. K. Chambers, …, H. Nakayama. 2012. Binding of curcumin to senile plaques and cerebral amyloid angiopathy in the aged brain of various animals and to neurofibrillary tangles in Alzheimer's brain. *J. Vet. Med. Sci.* 74:51–57.
21. Mithu, V. S., B. Sarkar, …, P. K. Madhu. 2014. Curcumin alters the salt bridge-containing turn region in amyloid β(1–42) aggregates. *J. Biol. Chem.* 289:11122–11131.
22. Porat, Y., A. Abramowitz, and E. Gazit. 2006. Inhibition of amyloid fibril formation by polyphenols: structural similarity and aromatic interactions as a common inhibition mechanism. *Chem. Biol. Drug Des.* 67:27–37.
23. Garai, K., B. Sahoo, …, S. Maiti. 2007. Zinc lowers amyloid-β toxicity by selectively precipitating aggregation intermediates. *Biochemistry.* 46:10655–10663.
24. Watt, N. T., I. J. Whitehouse, and N. M. Hooper. 2010. The role of zinc in Alzheimer's disease. *Int. J. Alzheimers Dis.* 2011:971021.
25. Tsvetkov, P. O., A. A. Kulikova, …, A. A. Makarov. 2010. Minimal Zn^{2+} binding site of amyloid-β. *Biophys. J.* 99:L84–L86.
26. Danielsson, J., R. Pierattelli, …, A. Gräslund. 2007. High-resolution NMR studies of the zinc-binding site of the Alzheimer's amyloid β-peptide. *FEBS J.* 274:46–59.
27. Zirah, S., S. A. Kozin, …, S. Rebuffat. 2006. Structural changes of region 1–16 of the Alzheimer disease amyloid β-peptide upon zinc binding and in vitro aging. *J. Biol. Chem.* 281:2151–2161.
28. Petkova, A. T., W. M. Yau, and R. Tycko. 2006. Experimental constraints on quaternary structure in Alzheimer's β-amyloid fibrils. *Biochemistry.* 45:498–512.
29. Mithu, V. S., B. Sarkar, …, P. K. Madhu. 2011. Zn^{2+} binding disrupts the Asp^{23}-Lys^{28} salt bridge without altering the hairpin-shaped cross-β structure of Aβ(42) amyloid aggregates. *Biophys. J.* 101:2825–2832.
30. Colvin, M. T., R. Silvers, …, R. G. Griffin. 2015. High resolution structural characterization of Aβ42 amyloid fibrils by magic angle spinning NMR. *J. Am. Chem. Soc.* 137:7509–7518.
31. Sengupta, P., J. Balaji, and S. Maiti. 2002. Measuring diffusion in cell membranes by fluorescence correlation spectroscopy. *Methods.* 27:374–387.
32. Sengupta, P., K. Garai, …, S. Maiti. 2003. Measuring size distribution in highly heterogeneous systems with fluorescence correlation spectroscopy. *Biophys. J.* 84:1977–1984.
33. Metz, G., X. L. Wu, and S. O. Smith. 1994. Ramped-amplitude cross-polarization in magic-angle-spinning NMR. *J. Magn. Reson. A.* 110:219–227.
34. Thakur, R. S., N. D. Kurur, and P. K. Madhu. 2006. Swept-frequency two-pulse phase modulation for heteronuclear dipolar decoupling in solid-state NMR. *Chem. Phys. Lett.* 426:459–463.
35. Weingarth, M., D. E. Demco, …, P. Tekely. 2009. Improved magnetization transfer in solid-state NMR with fast magic angle spinning. *Chem. Phys. Lett.* 469:342–348.
36. Morcombe, C. R., and K. W. Zilm. 2003. Chemical shift referencing in MAS solid state NMR. *J. Magn. Reson.* 162:479–486.
37. Sengupta, P., K. Garai, …, S. Maiti. 2003. The amyloid β peptide (Aβ(1–40)) is thermodynamically soluble at physiological concentrations. *Biochemistry.* 42:10506–10513.
38. Park, S. Y., H. S. Kim, …, D. Sul. 2008. Curcumin protected PC12 cells against β-amyloid-induced toxicity through the inhibition of oxidative damage and tau hyperphosphorylation. *Food Chem. Toxicol.* 46:2881–2887.
39. Thapa, A., B. C. Vernon, …, E. Y. Chi. 2013. Membrane-mediated neuroprotection by curcumin from amyloid-β-peptide-induced toxicity. *Langmuir.* 29:11713–11723.
40. Culbertson, C. T., S. C. Jacobson, and J. Michael Ramsey. 2002. Diffusion coefficient measurements in microfluidic devices. *Talanta.* 56:365–373.
41. Zhu, L., M. D. Kemple, …, F. G. Prendergast. 1995. N-terminus and lysine side chain pKa values of melittin in aqueous solutions and micellar dispersions measured by ^{15}N NMR. *Biochemistry.* 34:13196–13202.
42. Jaroniec, C. P., B. A. Tounge, …, R. G. Griffin. 2001. Frequency selective heteronuclear dipolar recoupling in rotating solids: accurate ^{13}C-^{15}N distance measurements in uniformly ^{13}C,^{15}N-labeled peptides. *J. Am. Chem. Soc.* 123:3507–3519.

43. Benilova, I., E. Karran, and B. De Strooper. 2012. The toxic Aβ oligomer and Alzheimer's disease: an emperor in need of clothes. *Nat. Neurosci.* 15:349–357.

44. Walsh, D. M., and D. J. Selkoe. 2007. Aβ-oligomers—a decade of discovery. *J. Neurochem.* 101:1172–1184.

45. Ono, K., M. M. Condron, and D. B. Teplow. 2009. Structure-neurotoxicity relationships of amyloid β-protein oligomers. *Proc. Natl. Acad. Sci. USA.* 106:14745–14750.

46. Noy, D., I. Solomonov, …, I. Sagi. 2008. Zinc-amyloid β interactions on a millisecond time-scale stabilize non-fibrillar Alzheimer-related species. *J. Am. Chem. Soc.* 130:1376–1383.

47. Prade, E., H. J. Bittner, …, B. Reif. 2015. Structural mechanism of the interaction of Alzheimer disease Aβ fibrils with the non-steroidal anti-inflammatory drug (NSAID) Sulindac sulfide. *J. Biol. Chem.* 290:28737–28745.